COHERENCE CHARACTERISTICS OF PRESSURE FLUCTUATIONS ON HEMISPHERICAL DOME

Yuan-Lung Lo[1] and Tzu-Ting Hsiao[2]

[1] *Assistant Professor, Department of Civil Engineering, Tamkang University, Tamsui, New Taipei City 25137, Taiwan, yllo@mail.tku.edu.tw*
[2] *Graduate Student, Department of Civil Engineering, Tamkang University, Tamsui, New Taipei City 25137, Taiwan*

ABSTRACT

Two systematic wind tunnel tests were conduct to investigate coherence characteristics of fluctuating wind pressures along the meridian on hemispherical domes due to Reynolds number effect and roof curvature effect. Reynolds number was first alternated from 6.6×10^4 to 1.9×10^6 under smooth and boundary layer flows. Root-coherences with respect to frequency and location were calculated to show how the Reynolds number effect changes the coherence distribution, especially when in approaching turbulent flows. Secondly, the roof curvature of the hemispherical dome was changed by f/D (height/span) from 0.5 to 0.1 to see the roof curvature effect. A modified form proposed by Hui et al (2009) was applied to present a more compact observation in a parametric study way rather than by Davenport's proposed. It was finally concluded that not only the location of the pressure but also the distance between two taps, can significantly determine the distribution features of coherences.

KEYWORDS: HEMISPHERICAL DOME, PRESSURE FLUCTUATION, COHERENCE

Introduction

Large span roof structures are common designs for various structures in a modern society, such as sport stadiums, coal/oil storage, museums, or certain symbolic, religious structures. Rather than seismic loads, what it may concern in this kind of structures is usually its curved geometry over a very large span, which may highly raise its sensitivity to wind loads. [Maher (1965)] first conducted measurements of mean wind pressures on hemispherical domes with various height-span ratios. He indicated that the drag force coefficient is less sensitive when Reynolds number is larger than 1.4×10^6. [Toy et al (1983)] then conducted similar experiments by alternating the approaching turbulences. Results showed that the increasing approaching turbulence impels the movement of separation and reattachment points along the dome surface. [Taylor (1991)] continued to indicate that under a turbulent flow, say turbulence intensity equals 15% or larger, the characteristics of wind pressures remain consistent when Reynolds number is larger than 1.7×10^5, which is an applicable operational value in most of tunnel tests. [Ogawa et al (1991)] investigated mean and R.M.S. wind pressures and spectrum characteristics of three hemispherical domes in laminar and turbulent flows. He gave the idea that dividing the dome roof into three zones: frontier zone, apex and side zone, and wake zone. He also proposed conventional models for approximations of power spectra and cross spectra. [Letchford and Sarkar (2000)] investigated the effect of surface roughness on the pressure distributions and on the overall drag and lift forces. [Uematsu and Tsuruishi (2008)] proposed a computer-assisted wind load

evaluation system for the design of roof cladding of hemispherical domes based on artificial neural network theory. The statistics of mean, R.M.S., skewness and kurtosis of wind pressures were computed and stored in the database. Non-Gaussian time series of wind pressures could be numerically simulated for wind load estimates based on FFT technique.

Among the aforementioned literatures, only few were given in describing the behavior of coherences of wind pressures. The exponential decaying coherence form proposed by [Davenport (1961)] was convenient and commonly applied for estimating co-coherences between any two fluctuating wind speeds. Nevertheless, [Ogawa et al (1991)] and [Uematsu et al (2008)] adopted another formula, an exponential amplitude multiplied by a cosine phase, to better approximate co-coherences. [Hui et al (2009)] simply modified the exponential decaying form by adding a coefficient to approach the non-unity coherence value at zero frequency for root coherences instead of co-coherences. [Lo and Kanda (2012)] indicated that a universal form is insufficient to represent all cross spectra, whether in the upstream region or downstream region. Similar qualitative discussion was also given by [Sun et al (2011)].

In this study, Reynolds number effect and roof curvatures are taken into considerations two most important factors for coherence characteristics of wind pressures on hemispherical domes. To well describe the characteristics of coherences, co-coherences are decomposed to root-coherences and phases. Hui's simple model is applied in this study for the parametric identification of root-coherences. In light of the past works on dome issues, it is believed worthy to accumulate more detailed data on aerodynamics of hemispherical domes for proper design purposes of wind loads.

Wind Tunnel Test on Surface Pressure Measurements

Reynolds number and roof curvature effects are individually conducted in two simulation settings of wind tunnel tests.

Wind Tunnel Tests for Reynolds Number Effects

Two flows, smooth and turbulent flow are simulated in a 24.0 m (length) × 4.0 m (width) × 2.6 m (height) boundary layer wind tunnel for the investigation of Reynolds number effects. For the smooth flow simulation in Figure 1, the base plate for installing the dome model is elevated 55.5 cm from the section ground to minimize the boundary layer effect. Turbulent profile remains a small and constant value of 1%~2% in Figure 2 where U_δ=11.8m/sec is selected only for explanations. For the turbulent flow, the suburban terrain with power law index α=0.27 is also shown in Figure 3. Profiles of mean wind speeds and turbulence intensities are shown in Figure 4 where the turbulence intensity varies from 18% to 25% at model heights. The boundary layer height, δ, is 140 cm and U_δ=9.9 m/sec.

Three acrylic hemispherical models with diameters of 120 cm, 50 cm, and 20 cm are installed sequentially; the corresponding Reynolds number varies from 6.6×10^4 to 1.9×10^6 by the definition of $R_e=U_HD/\upsilon$ where U_H is the mean wind speed at the model heights, D is the characteristic length of the model, usually the diameter of the hemisphere, and υ is the air density. The blockage percentages of projective areas of models are calculated to be 5.4%, 0.9%, and 0.15% respectively, which may be considered acceptable for wind tunnel tests.

The coordinate system of the model is indicated as Figure 5. Pressure taps are arranged along the meridian parallel to the direction of approaching wind. Instantaneous wind pressures are sampled simultaneously by a ZOC pressure scanner system at frequency of 300 Hz. Table 1 shows the basic information of testing models and its corresponding Reynolds numbers. Pressures through the scanner system are then processed by numerical correction of signal distortion based on inverse-FFT techniques.

Figure 1: Photo of Smooth Flow Simulation Setting

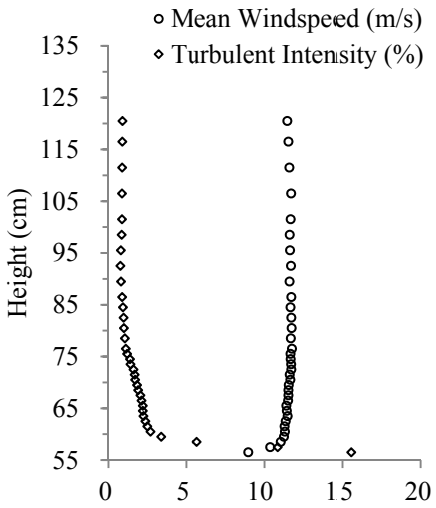

Figure 2: Distributions of Mean Windspeed and Turbulent Intensity Profiles of Smooth Flow

Figure 3: Photo of Turbulent Flow Simulation Setting

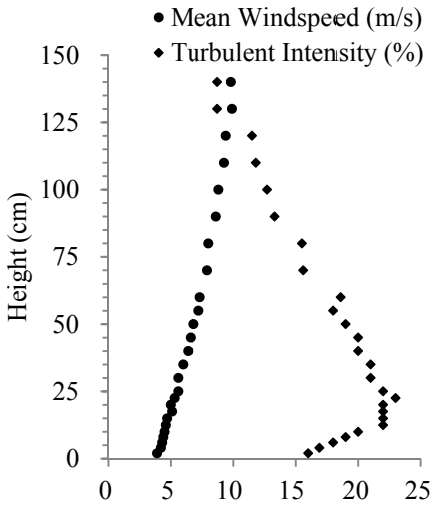

Figure 4: Distributions of Mean Windspeed and Turbulent Intensity Profiles of Turbulent Flow

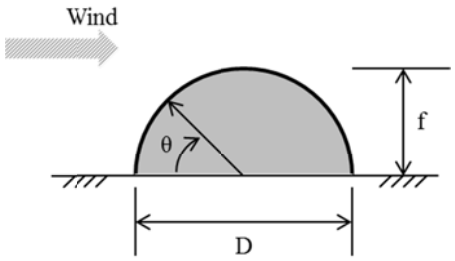

Figure 5: Coordinate System of Dome Model

Table 1: Basic Information of Analysis Cases for Reynolds number effects

Dome (Diameter in cm)	Reynolds Number	
	Smooth	Turbulent
S (D=20)	6.57×10^4 1.05×10^5 2.17×10^5	6.74×10^4 1.11×10^5 1.58×10^5
M (D=50)	4.24×10^5 6.16×10^5 8.09×10^5	2.73×10^5 4.33×10^5 6.06×10^5
L (D=120)	1.06×10^6 1.60×10^6 1.96×10^6	1.02×10^6 1.41×10^6 1.80×10^6

Wind Tunnel Tests for Roof Curvature Effects

Roof curvature effects are conducted in a turbulent flow with Reynolds number in the 10^5 range. A suburban terrain with power law index 0.27 is simulated in a 15.6 m (length) ×

1.8 m (width) × 1.8 m (height) boundary layer wind tunnel. Figure 6 shows the normalized mean wind profile and the turbulence intensity profile.

The roof curvature effects are examined by investigating the ratio of the roof height to the diameter of the hemispherical dome model. The diameter of models is fixed 30 cm while span heights are alternated to have 6 cases, which are f/D=0.1, 0.2, 0.3, 0.4, and 0.5. Vinyl tubes for pressure measurements are arranged along the meridian parallel to the wind direction. Mean wind speed at the height of the models is varying from 5.1 m/sec to 7.5 m/sec so that the range of Reynolds number is 1.1×10^5~1.6×10^5. According to [Cheng et al (2009)], when the turbulence intensity of approaching wind is high enough (>18%~20%), the Reynolds number effect is less significant when it is in the 10^5 range. Therefore in investigating the roof curvature effect, the Reynolds number effect can be remained unchanged. Table 2 shows the basic information of this part of wind tunnel tests.

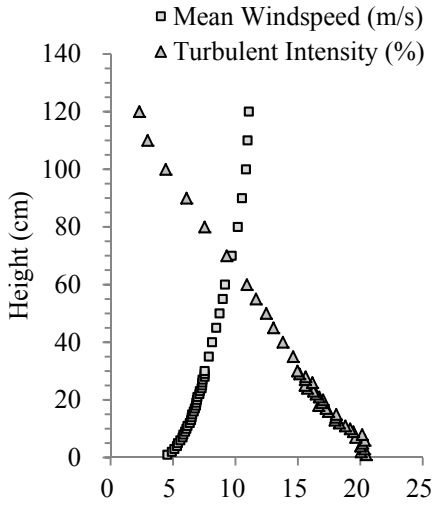

Figure 6: Distributions of Mean Wind Speed and Turbulent Intensity Profiles of Turbulent Flow (for Roof Curvature Effects)

Table 2: Basic Information of Analysis Cases for Roof Curvature Effects

	f/D (height/span)				
	0.1	0.2	0.3	0.4	0.5
Re	1.10	1.23	1.34	1.40	1.56
Unit: $\times10^5$					

Coherence Form and Its Parametric Identification Model

Coherence Form

In general, design wind loads of a structure can be obtained through the integration of the following equation,

$$S_F(f)=\sum_{i=1}^{m}\sum_{j=1}^{m}X_jX_iA_jA_iS_{pij}(f) \tag{1}$$

where f is frequency in Hertz; i, j represent two locations of pressures; X_i and X_j are structural mechanical functions at i and j; A_i and A_j are representative areas at i and j; $S_{pij}(f)$ is the cross spectrum of fluctuating pressures between i and j. Cross spectrum can be related to the following equation where co-coherence function is defined.

$$Coh_{ij}(\Delta s,f)=C_{ij}(\Delta s,f)/\sqrt{S_{pi}(f)\cdot S_{pj}(f)}=R_{ij}(\Delta s,f)\cdot e^{\sqrt{-1}\cdot\theta_{ij}(\Delta s,f)} \tag{2}$$

Δs is the net distance between i and j; $C_{ij}(\Delta s, f)$ is the co-spectrum part of $S_{pij}(f)$. $S_{pi}(f)$ and $S_{pj}(f)$ are power spectra of i and j. R_{ij} and θ_{ij} are root-coherence and phase decomposed from co-coherence. Therefore, from Equation (2), to achieve appropriate design wind loads, fine estimation of each component is essential, including the coherence component.

Parametric Identification Model for Root-coherence

To properly describe the coherence features, an exponential decaying form of co-coherence proposed by [Davenport (1961)] may need further modification, for instance, with coefficients to fit values at zero frequency. [Hui (2009)] therefore proposed a simple modified form with two coefficients for approximating root-coherences instead of co-coherences:

$$R_{ij}(\Delta s, f) = K \cdot \exp(-C \cdot \frac{f \Delta s}{U_H}) \tag{3}$$

In Equation (3), a decaying coefficient, C, approaches the decaying trend of the whole distribution and a modification coefficient, K, lowers the root-coherence value to a non-unity value at zero frequency. In this study, coefficients C and K varied with the Reynolds number and roof curvature effects are identified by least square method and plotted for qualitative investigations. Figure 7 shows an identification example of two coefficients. The distance between two pressures is represented as Δs or Δθ according to the coordinate system shown in Figure 5. However, coherences between two distant pressures may be meaningless so that only neighboring pressures are concerned in this paper.

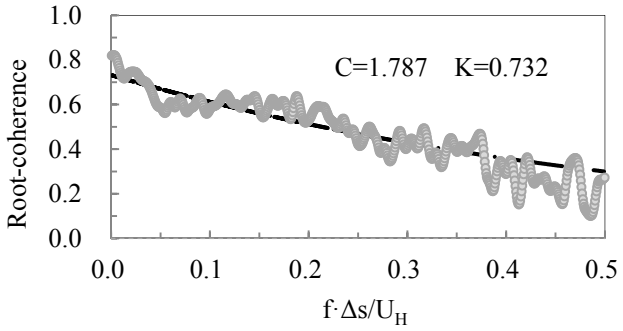

Figure 7: Example of Coefficient Identification of Root-coherence

Results and Discussions

Reynolds Number Effects-Smooth Flow

Reynolds number effects on root-coherences under smooth flows are investigated through the identified coefficients of Equation (3). For a hemispherical dome under smooth flows, laminar flow attaches the upstream area of the roof and then forms a shear layer flow along the surface. When the kinetic balance of viscosity force and inertia force cannot be maintained, shear layer flow separates from the surface and then forms wakes in the downstream area. In this study, separation point in lower Reynolds number cases is indicated around 80° ~ 90°. As Reynolds number increases, the separation point moves forward to 110° ~ 120°. Similar movement of separation point can be indicated in cases under turbulent flows.

Figure 8 shows the identified coefficients, C and K, of root-coherences between two pressures in 10° along the meridian. Scattering distribution is generally indicated in Figure 8 however root-coherences near and after separation point show much more significant scattering feature. For coefficient C, it seems difficult to give a good qualitative description when Reynolds number increases or when the root-coherence moves from upstream to

downstream. For coefficient K, the frontier area of the dome, where the horse vortex is considered to occur, has less-than-unity value at zero frequency and so does the area after the separation point occurs. It is also difficult to distinguish the Reynolds number effects from coefficient K; however, it can be indicated that as the interval of two pressures increases, almost the root-coherences on the whole surface have non-unity values at zero frequency.

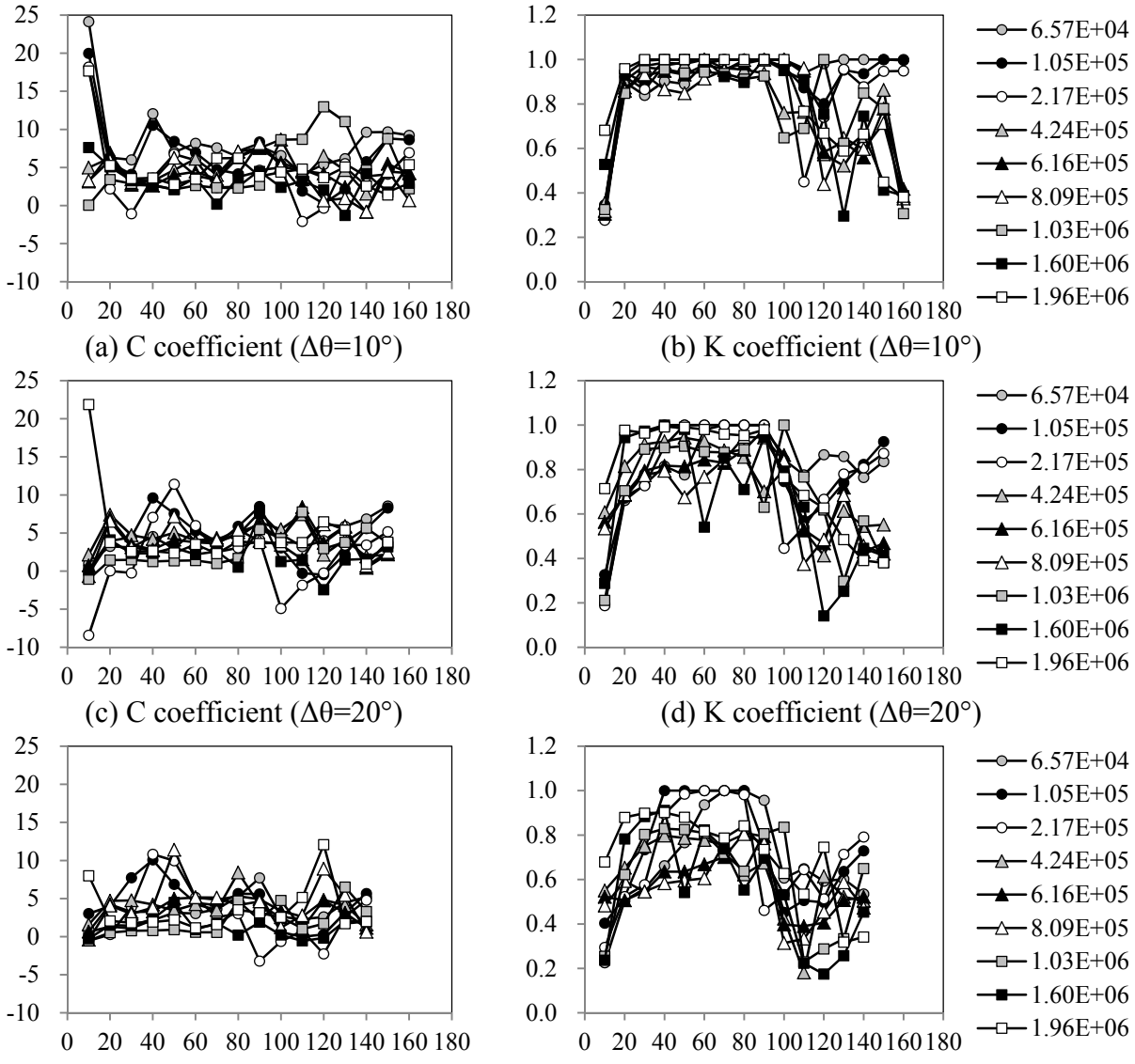

(a) C coefficient (Δθ=10°) (b) K coefficient (Δθ=10°)

(c) C coefficient (Δθ=20°) (d) K coefficient (Δθ=20°)

(e) C coefficient (Δθ=30°) (f) K coefficient (Δθ=30°)

Figure 8: Identification Results of Coefficients for Cases in Smooth Flows

Reynolds Number Effects-Turbulent Flow

Root-coherences under turbulent flows are investigated from Figure 9. Compared to Figure 8, cases under turbulent flows have clearer features in both identified coefficients. Similar to smooth flows, Reynolds number effects are not apparently indicated; however the scattering feature is reduced than that under smooth flows. As interval increases from Figure 9(a), 9(c) to 9(e), distribution feature changes slightly. In Figure 9(a), the area when positive pressures turn into negative pressures and the area near the separation point can be indicated local extremes of coefficients C and K; while in Figure 9(e), local extremes seem not follow the same observations. Coefficient K less than unity is generally seen along the meridian. To

further investigate the Reynolds number effects, the cases with Reynolds number larger than 10^6 are slightly differ from those under 10^6 among Figure 9(b), 9(d), and 9(f).

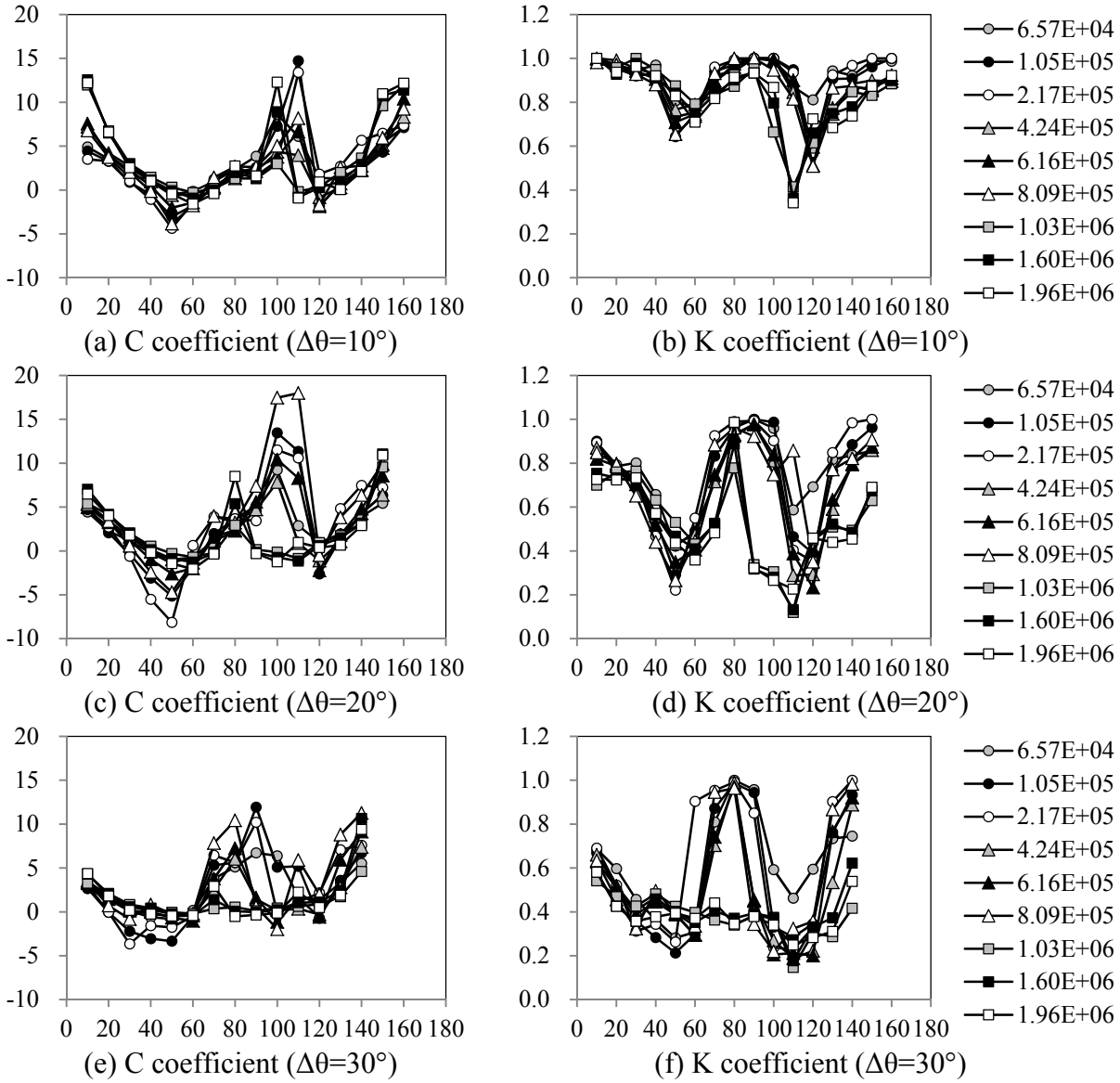

(a) C coefficient (Δθ=10°) (b) K coefficient (Δθ=10°)

(c) C coefficient (Δθ=20°) (d) K coefficient (Δθ=20°)

(e) C coefficient (Δθ=30°) (f) K coefficient (Δθ=30°)

Figure 9: Identification Results of Coefficients for Cases in Turbulent Flows

Roof Curvature Effects

Roof curvature effects are examined through the observation of coefficients C and K of Equation (3). In this case, Δθ between two pressures is different from domes. For instance, Δθ is 9° because there can only be installed 19 pressure taps along the meridian dividing to totally 20 pressures for f/D=0.1 dome. For f/D=0.2 dome, Δθ is about 6.42°; for f/D=0.3~0.5 domes, Δθ is 6°. Therefore, in Figure 10(a) and 10(b) shows the cases with one interval between two pressures and Figure 10(c) and 10(d) the cases with two intervals.

The Reynolds numbers in Figure 10 is about 1.1×10^5~1.6×10^5, whose distribution features are indicated similar to the cases 1.05×10^5 and 2.17×10^5. Unlike Figure 8 and Figure 9, Figure 10 shows quite distinct differences when f/D changes, which explains the roof curvature effect plays a more important factor than Reynolds number on coherences. Local extremes can be indicated near the separation point and the very upstream area. As f/D

increases, the variation is more distinct. It may be recommended to find a polynomial form to represent such effects in terms of f/D, instead of R_e.

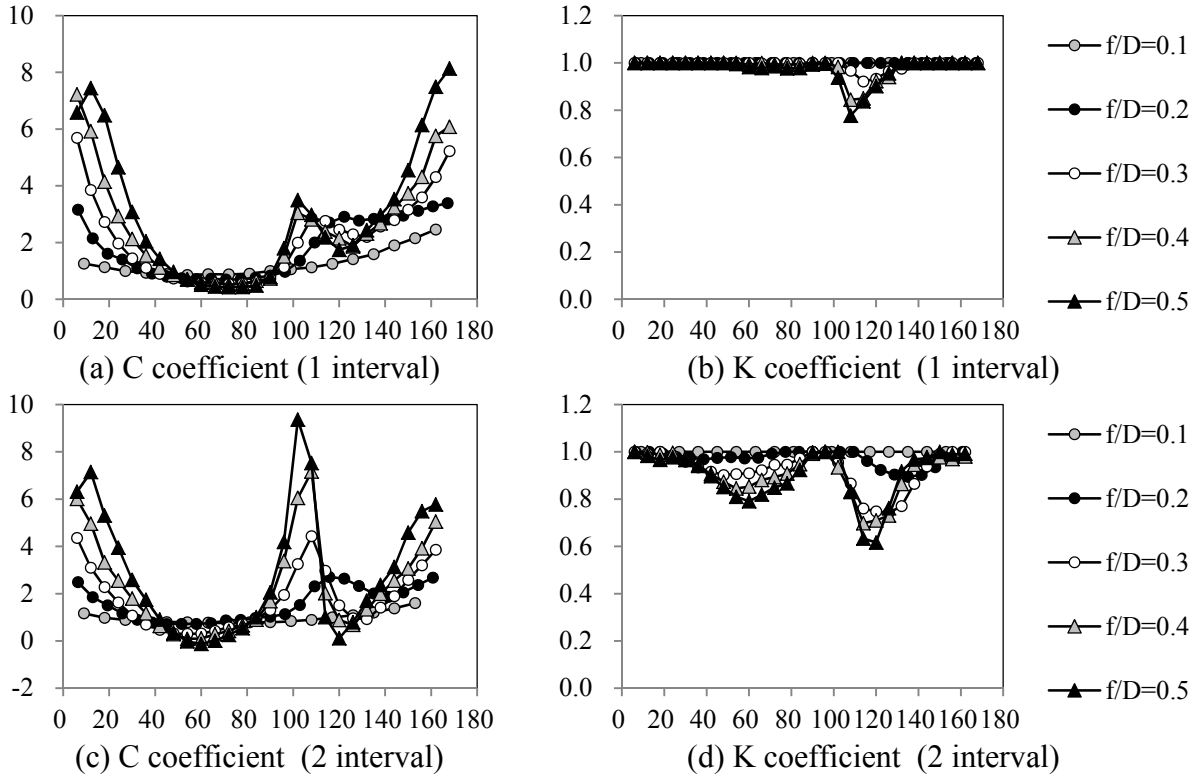

(a) C coefficient (1 interval) (b) K coefficient (1 interval)

(c) C coefficient (2 interval) (d) K coefficient (2 interval)

Figure 10: Identification Results of Coefficients for Roof Curvature Effects

Conclusions

Root-coherence varies with the location and the difference between two taps. In examining results of Reynolds number effects, rather than Reynolds number, approaching turbulence by simulated turbulent flow plays a more significant role. However, compared to Reynolds number effects, distribution of root-coherence seems more related to roof curvature effects. As the ratio of height to span, f/D, increases, the variations of fitting coefficients become clearer along the meridian. The interval between two pressures can even enhance the feature.

From analyzed results, a universal root-coherence formula is once again proved insufficient. In general, root-coherences vary significantly at lower frequency ranges, say less than 50Hz, which is within the sensitive range if scaled to a real structural dimension. Although the modified exponential model proposed by Hui can approach the non-unity value at zero frequency, the decaying form may be the only distribution type for different locations. In order to well estimate design wind loads, an advanced formula for describing cross spectra of fluctuating wind pressures, including the root-coherence and furthermore the phase, should be attempted in the next stage.

References

Cheng, C. M. and Fu, C. L. (2009), Characteristics of Wind Loads on a Hemispherical Dome in Smooth Flow and Turbulent Boundary Layer Flow, Journal of Wind Engineering and Industrial Aerodynamics, 98, 328–344

Davenport, A. G. (1961), Spectrum of Horizontal Gustiness near the Ground in High Winds, Journal of Royal Meteorological Society, 87, 194–211

Lo, Y. L. and Kanda, J. (2012), Cross Spectra of Wind Pressures on Domed Roofs in Boundary Layer Wind Tunnel, Proceedings of the Seventh International Colloquium on Bluff Body Aerodynamics and Applications, Shanghai, China, September 2-6, 2012

Hui, M.C.H., Larsen, A. and Xiang, H.F., (2009), "Wind turbulence characteristics study at the Stonecutters Bridge site : Part II: Wind power spectra, integral length scales and coherences", Journal of Wind Engineering and Industrial Aerodynamics, Vol. 97, pp. 48–59

Ogawa, T., Nakayama, M., Murayama, S., and Sasaki, Y. (1991), Characteristics of Wind Pressures on Basic Structures with Curved Surfaces and Their Response in Turbulent Flow, Journal of Wind Engineering and Industrial Aerodynamics, 38, 427–438

Qiu, Y., Sun, Y., Wu Y., (2011), Power Spectra of Fluctuating Wind Pressures on Spherical Domes, Proceedings of 13th International Conference on Wind Engineering, Amsterdam

Uematsu, Y. and Tsuruishi, R. (2008), Wind Load Evaluation System for the Design of Roof Cladding of Spherical Domes, Journal of Wind Engineering and Industrial Aerodynamics, 96, 2054–2066